

## Performance Enhancement of 2.5kW Induction Motor Drive Using Novel Hybridized Control Algorithm

Anyanime Tim Umoette<sup>1,\*</sup>, Ogbonnaya Inya Okoro<sup>2</sup>, and Chiweta E. Abunike<sup>2</sup>

<sup>1</sup>Dept. of Elect/Elect Engineering, Akwa Ibom State University, Ikot Akpaden, Nigeria

<sup>2</sup>Dept. of Elect/Elect Engineering, Michael Okpara Uni. of Agriculture, Umudike, Nigeria

\*Corresponding author: [libertycoast@yahoo.com](mailto:libertycoast@yahoo.com),

**Abstract:** Speed control of a squirrel cage induction motor (SCIM) using a novel control algorithm with proportional integral derivative (PID), fuzzy logic (FL) controller, hybrid controller (FL-PID), and optimized hybrid controller (FL-PID-PSO) was designed, simulated, and analyzed in this paper. 2.5kW three-phase SCIM was considered, and decoupling of the flux and torque-producing components for separate control was done for the actual control of the SCIM drive. The motor drive was used to drive a constant load of 0% (0 Nm), 50% (7 Nm), and 80% (12 Nm) of the rated torque with a variable speed of 0 rpm, 15 rpm, and 30 rpm. It was observed that FL-PID-PSO gave the best speed performance compared to other controllers. The steady-state error, rise time, settling time, overshoot, and undershoot of the proposed model were 0.04 rpm, 0.01 sec, 0.02 sec, 0.06%, and 0%, respectively, when driving 12 Nm at intermittent speed. The improved speed performance of the proposed FL-PID-PSO controller can be used in robotics where high precision speed performance is required.

**KEYWORDS:** Fussy logic, hybrid controller, indirect field oriented control, induction motor, MATLAB/Simulink

Date of Submission: 02-08-2024

Date of acceptance: 13-08-2024

### I. INTRODUCTION

Speed control of induction motors (IM) is of great practical concern in many modern industrial operations where variable speed applications are required. This is because IM has to satisfy strict speed characteristics requirements with respect to economic benefits, acceptable range, and smoothness of control [1–8]. Industrial applications such as conveyors and robotics require variable-speed motoring modes, where different speed operations are carried out within the same system [26, 27, 28 and 39]. IM is always used for these applications because of its inherent characteristics, including driving the systems that is energies from renewable energy sources [17, 18, and 19]. Variable Refrigerant Flow (VRF) technology uses variable-speed drive applications to provide the needed comfort to occupants. It exhibits a 20–40% reduction in energy consumption if the speed of the IM driving devices is well managed and regulated. Modern chiller systems are driven by an IM-based variable speed drive for high efficiency, where the speed of the IM is regulated and controlled [9, 29, and 30].

Technologies have made it possible to achieve efficient speed control with vector control techniques along with artificial and hybrid controllers in variable applications [10–13]. Control of IM behavior has been developed over the years, tailored to a lot of modern industrial operations. For example, [4] revealed that adequate speed control is required for proper energy management and efficiency improvement in the central chiller system. In [11], dynamic response using a fuzzy logic controller (FLC) was compared with a proportional integral (PI) controller, which showed superior performance at low speed. [5] presented variable refrigerant flow (VRF) technology using variable speed drives. The results showed that the energy consumed by the VRF system was reduced by 40%. In [14], particle swarm optimization (PSO) was used to get an optimized value, while [15] proposed a novel hybrid control of IM based on the combination of direct torque control (DTC) and genetic algorithms. The control method showed good performance at only one operating speed. A novel search algorithm was proposed in [16] and [17] to improve the design of the FLC and FLC-PIC, respectively, for IM speed control. The proposed algorithm provides an easy approach for obtaining membership functions. The developed controller

provided the needed stability and good dynamic response under speed and mechanical load changes. [18] studied the different methodologies of IM drive control. The study showed that the speed, power, and efficiency of IM have been controlled by various techniques like frequency control, supply voltage control, and the multiple-stator winding method. Implementation of IFOC on an IM drive with PI control was presented in [2], and the results show a good dynamic response in intermittent loading operating conditions. [1] used a finite element analysis approach to obtain the dynamic performance of IM under intermittent loading conditions without control. The simulation results showed the effect of different loads on the speed performance of the motor. The study [9] proposed a control technique that analyzed three different inverter modes (square wave, asynchronous, and synchronous).

The simulation results of the cited literature show that sensitive parameters like rise time, settling time, speed error, undershoots, overshoots, steady-state error, and load torque ripple of the IM drives are still high, which will not be accepted in many industrial applications. Also, low-speed control of IM was not given the needed attention. Hence, speed control of an IM still requires more research recognition, which will be considered in this paper. The present study will focus on driving a 2.5kW squirrel cage IM (SCIM) on an intermittent basis of 0 rpm, 15 rpm, and 30 rpm. The SCIM will be subjected to 0%, 50%, and 80% of its rated load torque using different controllers (PID, FL, hybrid FL-PID, and hybrid FL-PID-PSO). The performance of these controllers will be assessed and compared. The study is expected to produce a SCIM model with improved speed and performance characteristics compared to previous literature. Moreover, the proposed control algorithm will lead to improvements in variable applications like chillers, VRF technology, cranes, and robotics [40-45]

## II. ANALYTICAL MODELLING OF SCIM

SCIM is an AC machine whose speed at loading conditions is always less than the synchronous speed, and it operates on the principle of electromagnetic induction. [1] and [19] analyzed the performance of SCIM in steady-state conditions [20] also outlined the design strategy for achieving the desired performance. A three-phase 2.5Kw SCIM is used in this study. The flux linkage equations of SCIM on the dq0 axis using the analytical method are given in equations (1)– (4):

$$\frac{d\psi_{qs}}{dt} = \omega_b [V_{qs} - \frac{w_e}{\omega_b} \psi_{ds} + \frac{R_s}{X_{Is}} (\psi_{mq} - \psi_{qs})] \quad (1)$$

$$\frac{d\psi_{ds}}{dt} = \omega_b [V_{ds} + \frac{w_e}{\omega_b} \psi_{qs} + \frac{R_s}{X_{Is}} (\psi_{md} - \psi_{ds})] \quad (2)$$

$$\frac{d\psi_{qr}}{dt} = \omega_b [V_{qr} - \frac{w_e - w_r}{\omega_b} \psi_{dr} + \frac{R_r}{X_{Ir}} (\psi_{mq} - \psi_{qr})] \quad (3)$$

$$\frac{d\psi_{dr}}{dt} = \omega_b [V_{dr} + \frac{w_e - w_r}{\omega_b} \psi_{qr} + \frac{R_r}{X_{Ir}} (\psi_{md} - \psi_{dr})] \quad (4)$$

Where

$$\psi_{mq} = X_{m1} \left[ \frac{\psi_{qs}}{X_{Is}} + \frac{\psi_{qr}}{X_{Ir}} \right] \quad (5)$$

$$\psi_{md} = X_{m1} \left[ \frac{\psi_{ds}}{X_{Is}} + \frac{\psi_{dr}}{X_{Ir}} \right] \quad (6)$$

$$X_{m1} = \frac{1}{\left( \frac{1}{X_m} + \frac{1}{X_{Is}} + \frac{1}{X_{Ir}} \right)} \quad (7)$$

By substituting the flux linkages, currents in d-axis and q-axis are given as:

$$i_{qs} = \frac{1}{X_{Is}} (\psi_{qs} - \psi_{mq}) \quad (8)$$

$$i_{ds} = \frac{1}{X_{Is}} (\psi_{ds} - \psi_{md}) \quad (9)$$

$$i_{qr} = \frac{1}{x_{lr}} (\Psi_{qr} - \Psi_{mq}) \tag{10}$$

$$i_{dr} = \frac{1}{x_{lr}} (\Psi_{dr} - \Psi_{md}) \tag{11}$$

Equation (12) and (13) represent the Electromagnetic torque and rotor speed respectively.

$$T_e = \frac{3}{2} \left(\frac{p}{2}\right) \frac{1}{\omega_b} (\Psi_{ds} i_{qs} - \Psi_{ds} i_{ds}) \tag{12}$$

$$\omega_r = \int \frac{p}{2J} (T_e - T_L) \tag{13}$$

Where  $p$  is the number of poles,  $J$  is the moment of inertia, is the flux linkage, is the reactance, is the stator resistance, and is the rotor resistance.

Also, equations (14) through (16) represent the three-phase stator voltages of SCIM.

$$V_a = \sqrt{2} V_{rms} \sin(\omega t) \tag{14}$$

$$V_b = \sqrt{2} V_{rms} \sin\left(\omega t - \frac{2\pi}{3}\right) \tag{15}$$

$$V_c = \sqrt{2} V_{rms} \sin\left(\omega t + \frac{2\pi}{3}\right) \tag{16}$$

### III. DESIGN OF CONTROL ALGORITHMS

Decoupling an SCIM is always tedious due to the interaction between the torque and fluxes, whose orientations are dependent on the operating conditions of the motor. DC machine-similar performance can be obtained in SCIM by decoupling torque and flux. In this paper, PID controllers and FL controllers are designed and hybridized to form a single controller. and the hybridized gain parameters are optimized using PSO to control

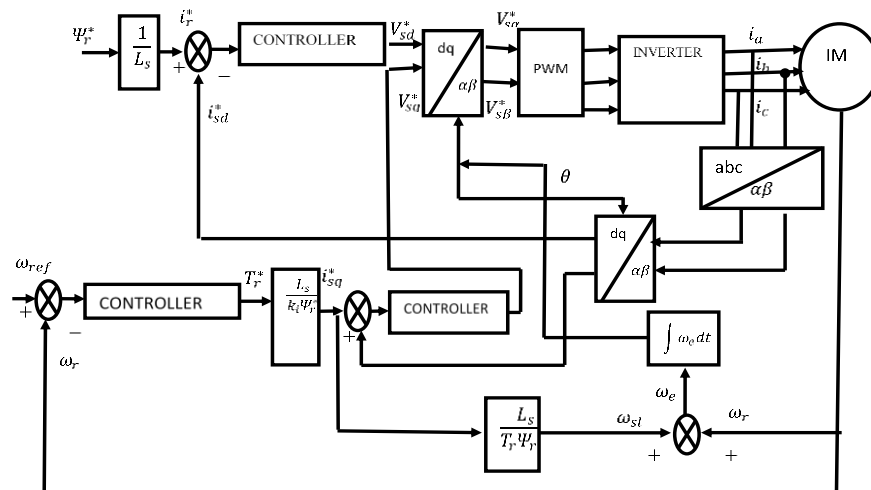


Figure 1. Block diagram of IFOC of SCIM [34]

the speed of the IM [33 and 34]. The following are noted in the design of the vector control: The reference direct – axis stator current  $i_{sd}^*$  depends on the reference flux  $\Psi_r^*$  which is chosen as 0.96 as shown in equation (17),  $L_m$  is the mutual inductance and Quadratic – axis reference stator current reference  $i_{sq}^*$  can be calculated from equation (18), where  $L_r$  is the rotor inductance,  $P$  is the number of poles.

$$i_{sd}^* = \frac{\Psi_r^*}{L_m} \tag{17}$$

$$i_{sq}^* = \frac{T_e^*}{K_i \psi_r^*} \quad (18)$$

$$\text{where } K_i = \frac{3pL_m}{4L_r}$$

The electromagnetic torque ( $T_e$ ), rotor speed ( $\omega_{sr}$ ), slip ( $\omega_{sl}$ ), rotor flux angle ( $\theta_e$ ) are respectively given as:

$$T_e = \frac{3}{2} \left( \frac{P}{2} \right) \frac{L_m}{L_r} \psi_r i_{qs} \quad (19)$$

$$\omega_{sr} = \frac{L_m R_r}{\psi_r L_r} i_{qs} \quad (20)$$

$$\omega_{sl} = \frac{L_m i_{sq}^*}{T_e \psi_r^*} \quad (21)$$

$$\theta_e = \int (\omega_r + \omega_{sl}) dt \quad (22)$$

Where  $L_m$  is mutual induction,  $\psi$  is flux linkage

. Coordinate transformation is obtained from equation (23)

(from figure 1), the obtained signal,  $\omega_{sr}$ , is added with rotor speed signal,  $\omega_r$ , to generate frequency signal,  $\omega_e$ , and rotor flux angle,  $\theta_e$

$$\theta_e = \theta_r + \theta_{sl} \quad (24)$$

The block diagram of indirect field-oriented control of an induction motor is shown in figure 1. The outputs of the Clark block are  $i_{\alpha}$  and  $i_{\beta}$ , and these signals serve as the inputs to the park transformation block. The position of the angular flux is required for computing the two component currents. The d-q currents are compared to the reference flux and torque. The flux command indicates the right rotor flux command forever speed reference within the nominal value. The inverse output of these transformations enters the inverter, which drives the motor at the required signal for the reference speed value and smooth speed control. The control algorithm provides inverter switching commands to achieve the desired speed at the motor shaft. The algorithm for indirect field oriented control can be summarized as follows:

The phase currents  $I_a$ ,  $I_b$  and  $I_c$  will be fed to clark transformation module which, will give two phase current components  $I_{\alpha}$  and  $I_{\beta}$  in stationary reference

The stationary currents will be transformed into rotating reference frame components  $I_d$  and  $I_q$  using the park transformation.

The rotor flux will be computed using:

$$\psi_r = \frac{L_m i_d}{1 + \tau_r} \quad (25)$$

Where  $\tau_r$  is the rotor time constant calculated from:

$$\tau_r = \frac{L_r}{R_r} \quad (26)$$

The rotor angle  $\theta_e$  will be computed from (24) and used for coordinate transformation. The actual motor speed will be computed using the reference speed and the error produced will be fed to the speed controller. The controller output is electromagnetic torque,  $T_e$ . The quadratic stator current components reference  $i_q$  and  $i_d$  will be computed from (17) and (18), respectively.  $i_q$  and  $i_d$  current reference will be converted into  $i_{\alpha}$  and  $i_{\beta}$  current reference in a stationary reference frame using park transformation. Also,  $i_{\alpha}$  and  $i_{\beta}$  will be converted into phase current reference  $i_a$ ,  $i_b$  and  $i_c$  by using inverse clark transformation that will be used in the motor drive. The Clarke transformation method transforms a three-phase system into a two-phase system (stationary reference frame). (27) and (28) are generated based on (14), (15), and (16).

$$V_{\alpha} = \frac{2}{3} V_a + \frac{1}{3} V_b - \frac{1}{3} V_c \quad (27)$$

$$V_{\beta} = \frac{1}{\sqrt{3}} V_b - \frac{1}{\sqrt{3}} V_c \quad (28)$$

Clarke transformation in matrix form and inverse clark transformation are respectively given as:

$$\begin{bmatrix} V_{\alpha} \\ V_{\beta} \end{bmatrix} = \frac{2}{3} \begin{bmatrix} 1 & 1/2 & -1/2 \\ 0 & \sqrt{3}/2 & -\sqrt{3}/2 \end{bmatrix} \begin{bmatrix} V_a \\ V_b \\ V_c \end{bmatrix} \quad (29)$$

$$\begin{bmatrix} V_d \\ V_q \end{bmatrix} = \begin{bmatrix} 1 & 0 \\ \frac{1}{2} & \frac{-\sqrt{3}}{2} \\ -\frac{1}{2} & \frac{\sqrt{3}}{2} \end{bmatrix} \begin{bmatrix} V_\alpha \\ V_\beta \end{bmatrix} \tag{30}$$

The transformation of the equations to rotating reference frame in direct and quadrature axis uses park transformation technique. This is expressed in equation (30)

$$\begin{bmatrix} V_d \\ V_q \end{bmatrix} = \begin{bmatrix} \cos \theta & \sin \theta \\ -\sin \theta & \cos \theta \end{bmatrix} \begin{bmatrix} V_\alpha \\ V_\beta \end{bmatrix} \tag{31}$$

three-phase system of stator and rotor are calculated as in equations (32) and (33)

$$\begin{bmatrix} i_\alpha \\ i_\beta \end{bmatrix} = \begin{bmatrix} \cos \theta & -\sin \theta \\ \sin \theta & \cos \theta \end{bmatrix} \begin{bmatrix} i_d \\ i_q \end{bmatrix} \tag{32}$$

$$\begin{bmatrix} i_a \\ i_b \\ i_c \end{bmatrix} = \frac{2}{3} \begin{bmatrix} 1 & 0 \\ -1/2 & -\sqrt{3}/2 \\ -1/2 & \sqrt{3}/2 \end{bmatrix} \begin{bmatrix} i_\alpha \\ i_\beta \end{bmatrix} \tag{33}$$

(33) represents the final value of the three-phase system that is emerging from the motor. This concept of transformation allows the speed control of SCIM to be possible.

### 3.1 Design of PID Controller

Figure 2 shows the block diagram of the PID controller. From Figure 3, the output of the PID controller,  $u(t)$ , constitutes the sum of three signals: the signal obtained by multiplying the error signal by a constant proportional gain,  $k_p$ ; the signal obtained by differentiating and multiplying the error signal by a constant derivative gain,  $k_d$ ; and the signal obtained by integrative control response. This approach has superior features like easy implementation and less computational effort [21,30, 31, and 36]. Defining  $u(t)$  as the controller output, the final form of the PID algorithm is from equation (34).

$$u(t) = k_p \cdot e(t) + k_i \int e(t)dt + k_d \frac{de(t)}{dt} \tag{34}$$

The tuning mechanism is designed using MATLAB software tools for deriving the transfer function of the complex SCIM and varying the PID parameters to control the speed of the motor. After a successful tuning of the controller using trial and error method, a fixed PID gains of  $k_i = 1.3$ ,  $k_p = 87.1$  and  $k_d = 0.004$  were realized to arrive at best dynamic performance.

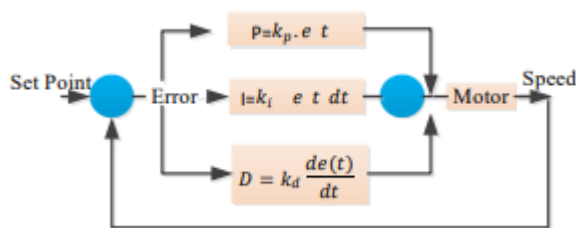


Figure 2. Block diagram of PID controller [31]

### 3.2 Design of Fuzzy Logic Controller

In the speed control of SCIM, which is the focus of this paper, a fuzzy logic controller (FLC) is used because of the nonlinear characteristics of SCIM [22, 23]. A rule that consists of ‘If-Then’ is created to define the behaviors of the system. These rules are likened to the human thought process, hence providing artificial intelligence to the system. Figure 4 shows the three-dimensional view of the control surface, where the range of error and change in error are [-50, 50] and [-30, 30], respectively. The proposed fuzzy logic design has seven

triangular membership functions for error, E, change in error, CE, and nine triangular membership functions for the output, U. The proposed fuzzy linguistic sets for membership functions of the input and output are Z = zero, PS = positive small, NB = negative big, PM = positive medium, and NM = negative. The choice of membership functions affects the design of a FLC. Membership functions are a curve that determines the value of the input signal to the fuzzy controllers medium, NVB = negative very big, PVB = positive very big, NS = negative small, PB = positive big.

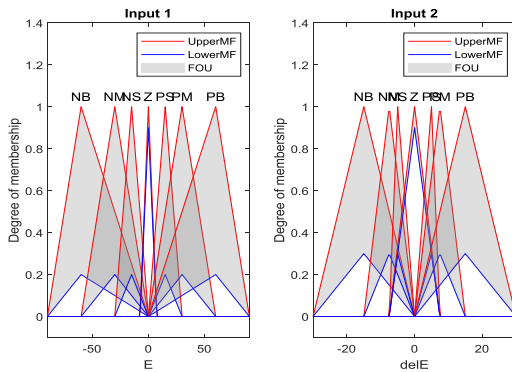


Figure 3. Membership functions of fuzzy logic controller

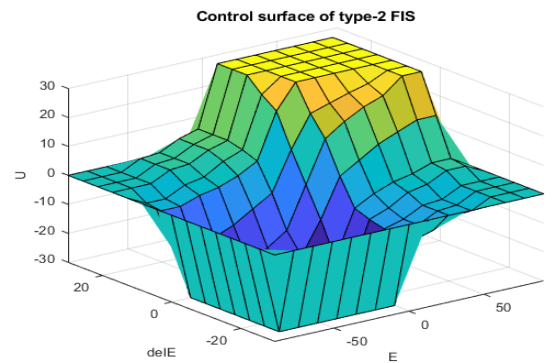


Figure 4. Three-dimensional plot of control surface

The membership functions used to fuzzify the FLC's two inputs and the plot are displayed in Figure 4 and Figure 4. The membership functions' points that need to be adjusted are c1 and c2 for output, du; a1 and a2 for error, e; and b1 and b2 for change in error, ce. The output's n1, n2, and n3 normalization parameters for the two inputs are as follows: As a result, nine parameters (n1, n2, n3, a1, a2, b1, b2, c1, c2) must be optimized for the design of FLC. Link between knowledge and inference mechanisms the relationship between the output and input. The fuzzy logic controller has two inputs and one output, with seven membership functions each. The combination of the two inputs will lead to forty-nine combinations, or forty-nine rules. The rules are presented in Table 1

Table 1: The Rule base of fuzzy logic controller

		e							
		NB	NM	NS	Z	PS	PM	PB	
ce	NB	NVB	NVB	NVB	NB	NM	NS	Z	du
	NM	NVB	NVB	NB	NM	NS	Z	PS	
	NS	NVB	NB	NM	NS	Z	PS	PM	
	Z	NB	NM	NS	Z	PS	PM	PB	
	PS	NM	NS	Z	PS	PM	PB	PVB	
	PM	NS	Z	PS	PM	PB	PVB	PVB	
	PB	Z	PS	PM	PB	PVB	PVB	PVB	

### 3.3 Design of Hybrid Speed Controller

The hybrid controller in this paper is the hybridization of PID and FLC, and it is used as a single controller to control the speed of the SCIM using the vector control technique. The hybrid model is shown in Figure 3, and its Simulink model is shown in Figure 5.

The inputs of the FLC are the error, E, and the change in error, CE, and the output of the FLC serves as an input (error signal) to the PID error signal. Due to the combination of the strengths of the two controllers, the hybrid controller offers a high level of system stability against load variations [17 , 32].

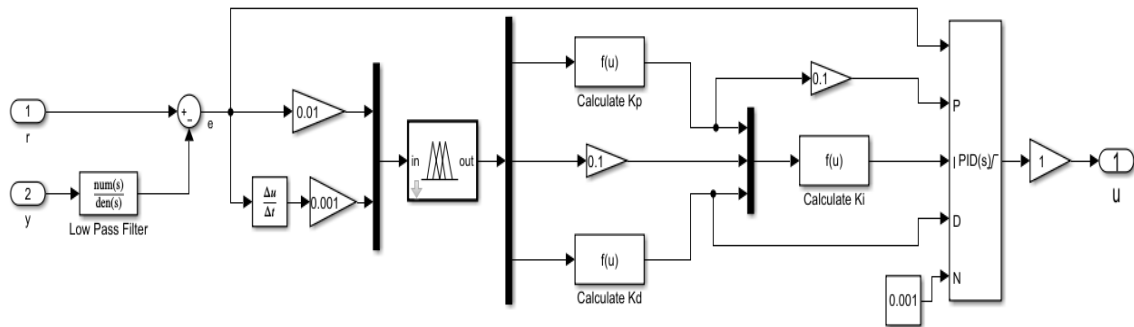


Figure 5. Simulink model of FLC- PID controller

### 3.4 Design of Particle Swarm Optimizer

Particle swarm optimization (PSO) optimizes an objective function by undertaking a population-based search. Figure 6. represents the general flow of PSO. The population consists of potential solutions, named particles, which are metaphors of birds in flocks. These particles are randomly initialized and freely fly across the multi-dimensional search space [13, 24, 25, and 26]. During flight, each particle updates its own velocity and position based on its best experience and the entire population. At each iteration, each of these particles modifies its velocity and position according to its own experience of flying and the experience of its neighbors through a communication network between the swarm members to find the best solution. The velocity and the position of each particle are respectively represented in the number, *n*, of iterations, as

$$V_i(k) = [V_{i1}(k), V_{i2}(k) \dots V_{in}(k)]^T \tag{35}$$

$$X_i(k) = [X_{i1}(k), X_{i2}(k) \dots X_{in}(k)]^T \tag{36}$$

At each iteration, the particle rushes to get the best local position based on its own memory. This is what distinguishes the PSO algorithm from the other algorithms and can be presented at each iteration. The local or personal best position of the particle up to time, *k*, is represented in equation 37.

$$P_{best}(k) = [P_{besti1}(k), P_{besti2}(k) \dots P_{bestin}(k)] \tag{37}$$

While the global best, which is the best solution of all the particles in the whole group is represented in equation (38)

$$G_{best}(k) = [G_{besti1}(k), G_{besti2}(k), G_{bestin}(k)] \tag{38}$$

After finding the best  $G_{best}$  and  $P_{best}$ , the particles modify their positions and velocity at time (*k*+1) according to:

$$V_i^{k+1} = wV_i^k + c_1r_1(P_{best_j} - S_i^k) + c_2r_2(g_{best_j} - S_i^k) \tag{39}$$

$$w = w_{max} - \frac{w_{max}-w_{min}}{iter_{max}} \times iter \tag{40}$$

Where  $V_i^k$  is the current velocity of agent *I* at iteration *k*,  $V_i^{k+1}$  is the updated velocity of agent *I*,  $r_1$  and  $r_2$  are random numbers uniformly distributed in [0,1],  $S_i^k$  is the current position of agent *I* at iteration *K*,  $p_{best}$  is  $p_{best}$  of agent *i*,  $g_{best}$  is  $g_{best}$  of agent *i*, *w* is weight function for velocity of agent *i*,  $c_1$  and  $c_2$  are positive constants, called cognitive and social parameters respectively,  $w_{max}$  is maximum weight,  $w_{min}$  is minimum weight,  $iter_{max}$

is maximum iteration number, *iter* is the current iteration number. Based on equation (40), an updated velocity can be calculated.

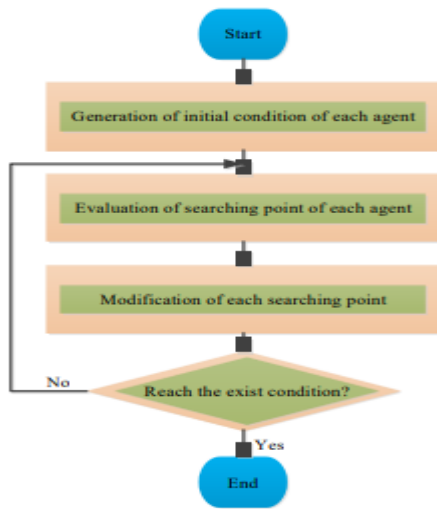


Table 2. SCIM parameter

Motor parameters	specification
voltage	460
Power	2.5kW
Frequency	50Hz
Rotor Resistance	0.228Ω
Stator Resistance	0.087Ω
Rotor Inductance	0.8 × 10 <sup>-3</sup>
Stator Inductance	0.8 × 10 <sup>-3</sup>
Mutual Inductance	0.0347H
Pole	4
Initial speed	1.662Kg <sup>m</sup> <sup>2</sup> 1440RPM

Figure 6. General flow chat of PSO [13, 38]

The current position can be modified as:

The general flow chart of PSO is shown in Figure 6. It can be described as follows:

Step 1: generation of the initial condition of each agent randomly within the allowable range, that is, the initial searching point and velocities of each agent. Pbest is the current searching point for each agent, and the best of Pbest is set to global best (gbest).

Step 2: Searching point of each agent evaluation. In this step, the objective function is calculated for each agent, and when the value is realized, the pbest is obtained, and the agent number with the best value is stored. (37) and (38) are used for the modification of the search point.

Step 3: If the desired value is reached, exit or go back to step 2.

From (35), the speed of each particle has three components, which are: momentum, a component towards the bird's self-best, and a component towards the global swarm's best. Also, adaptability and stability are the essential characteristics of the PSO method. The normalization parameters, de-normalization parameters, and parameters of the membership functions are improved by optimizing properly defined objectives or fitness functions [10]. The two inputs of the FLC, error (e) and change in error (ce), are represented in equations (41), (42) and (43)

$$e(t) = \omega_r^* - \omega_r \tag{41}$$

$$ce(t) = e(t) - e(t + 1) \tag{42}$$

$$f_e = \int_0^t (\omega_r^* - \omega_r) dt \tag{43}$$

The purpose of the optimization is to minimize the objective function of (43).

#### IV. DESIGN RESULTS AND DISCUSSION

This section will present the performance results of the SCIM using the different controllers (PID, FL, hybrid FL-PID, and hybrid FL-PID-PSO). The parameters of the tested motor are listed in Table 2. The design and simulation were carried out using the Simulink toolbox in MATLAB. The controllers were separately designed (as displayed in Figure 5) for the varying speed control of the motor on an intermittent basis of 0 rpm

(from 0-0.5 sec), the speed increases to 15 rpm (from 0.5–1 sec), and the speed further increases to 30 rpm (from 1-2 sec) for different percentages of its rated load (0Nm (0%), 7Nm (50%), and 12Nm (80%)). The speed, torque, and current responses of each controller were studied, analyzed, and compared in terms of steady-state error, rise time, settling time, overshoot, and undershoot. The simulation results are subdivided into the subsequent sections.

#### 4.1 Results under variable speed and constant load torque using PID controller

The speed performance of the SCIM drive with PID controller is presented in Figure 7. Simulation shows the good performance of IFOC using PID under variable speed and constant load operating conditions. Figure 7 shows that speed tracking is smooth and fast, this is quite recommended for this operating condition where there is a fast change in reference speed. This highlights a good transient response from the models. The speed response of the motor has an overshoot of 13.13% and an undershoot of 0% at no load. Also, the settling time, rise time, and steady state error are 0.2 sec, 0.04 s, and 1.03 rad/s, respectively. The corresponding electromagnetic torque and current response are shown in Figures. 8 and 9, respectively. In Figure. 9, each overshoot at every speed increase and settles after 0.2 s, while in Figure. 9, the overshoot at every increase in speed settles immediately after 0.05 sec. The overall performance parameter of this model is recorded in Table 3.

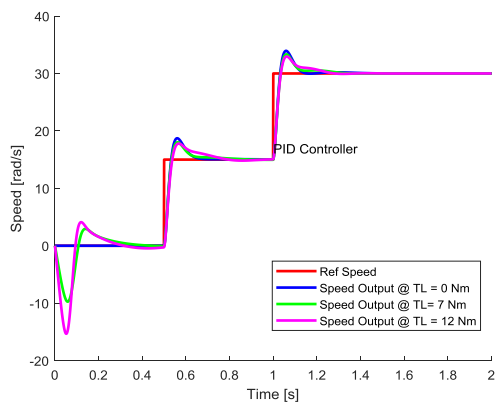


Figure 7. Speed response with PID controller

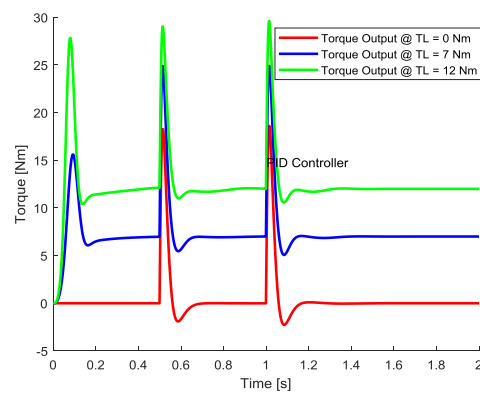


Figure 8. Torque response with PID controller

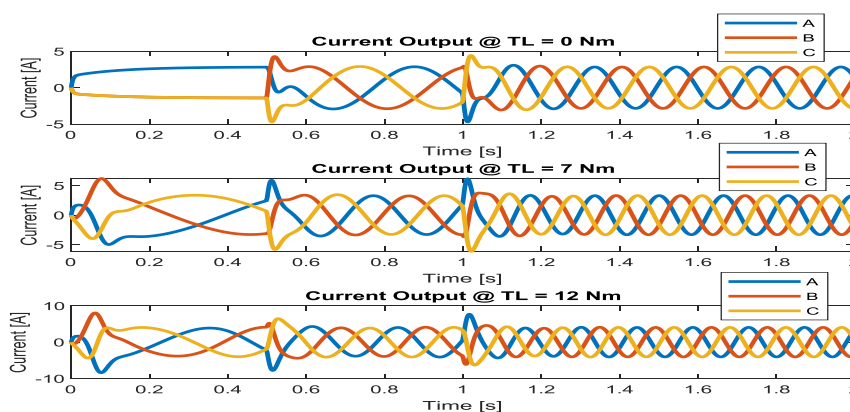


Figure 9. Current response with PID controller

4.2 Results under variable speed and constant load torque using Fuzzy logic controller

Figure 10 shows the speed performance of the SCIM with FLC at various load torques. As shown in Figure 10, it shows better speed performance when compared with the result of the PID controller. The speed tracking ability of this model is faster, and it displays better transient response ability. It has been shown according to Table 3 that a lesser value of steady state error, settling time, rise time, and overshoot in speed response. The motor speed response has an overshoot of 10.362% and an undershoot of 0% when driving at no load. Also, the settling time, rise time, and steady state error are 0.18 sec, 0.03 sec, and 0.5 rad/s, respectively. The corresponding electromagnetic torque and current response are shown in Figures 11 and 12, respectively.

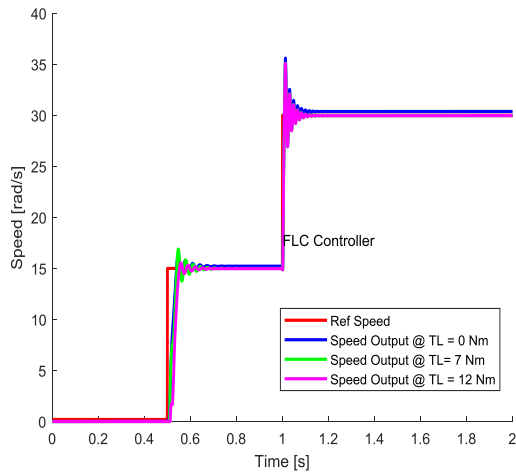


Figure 10.Speed response with FL controller

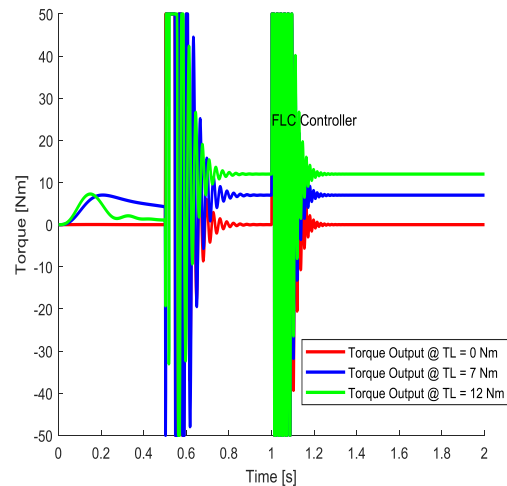


Figure 11.Torque response with FL controller

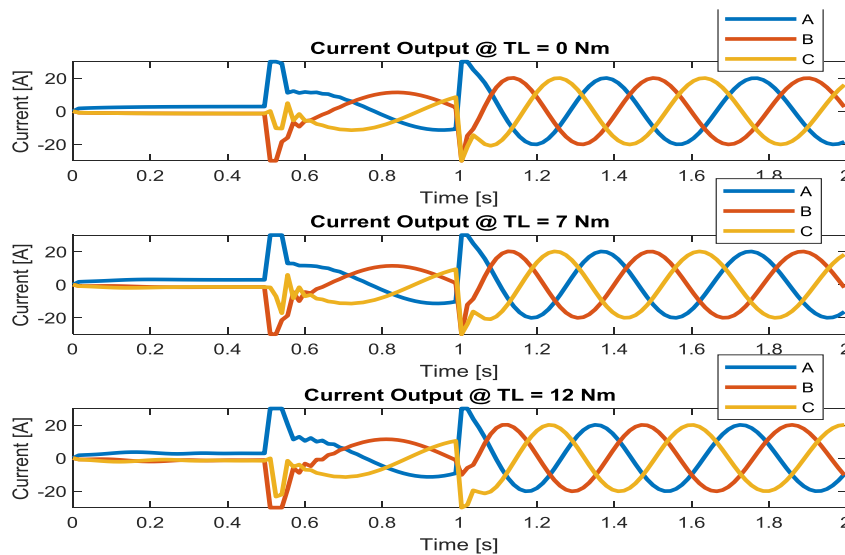


Figure 12.Current response with FL controller

Each torque response overshoots at every speed increase and settles after 0.3 sec, as seen in Figure 12. Also, there is an overshoot at every increase in speed value in Figure 13, which settles immediately after 0.03 sec..

**4.3 Results under variable speed and constant load torque using FL-PID controller**

Using the FL-PID controller, the speed response of SCIM is presented in Figure 13. There is a combined strength in this model, where the weaknesses of PID and FL controllers are eliminated. This results in better dynamic speed performance compared to what is available for FL and PID controllers. Speed characteristics in Figure 13 have overshoots of 9.87% and undershoots of 0% at no load. Also, the settling time, rise time, and steady state error are 0.17 sec, 0.026 sec, and 0.2 rad/s, respectively. There is an improvement in performance when compared to the dynamic performance of the motor with PID and FL controllers under this operating condition. The corresponding electromagnetic torque and current response are shown in Figures 14 and 15, respectively.

Each torque response overshoots at every increase in speed and settles after 0.1 sec in Figure 14, while Figure 15 shows that there is an overshoot of the current response at every increase in speed, which settles immediately after 0.02 sec.

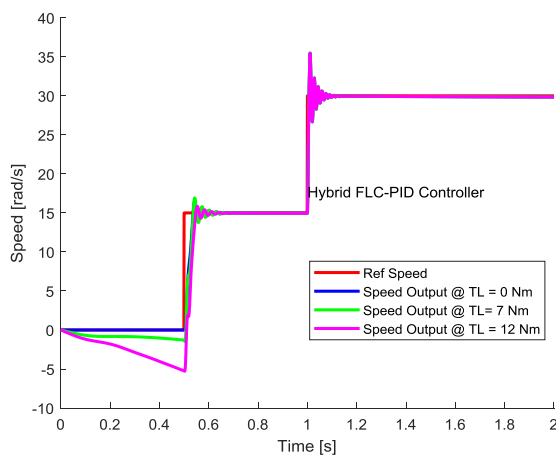


Figure 13. Speed response with FL-PID controller

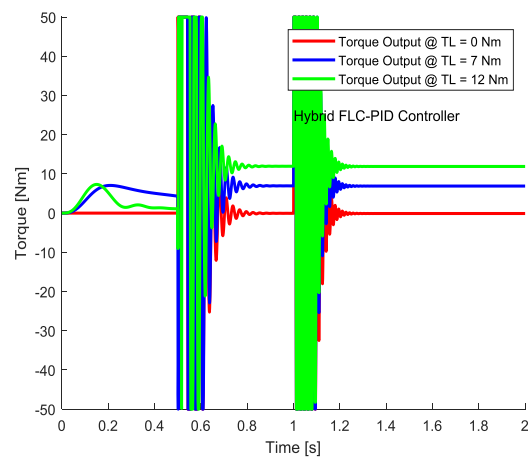


Figure 14. Torque response with FL-PID controller

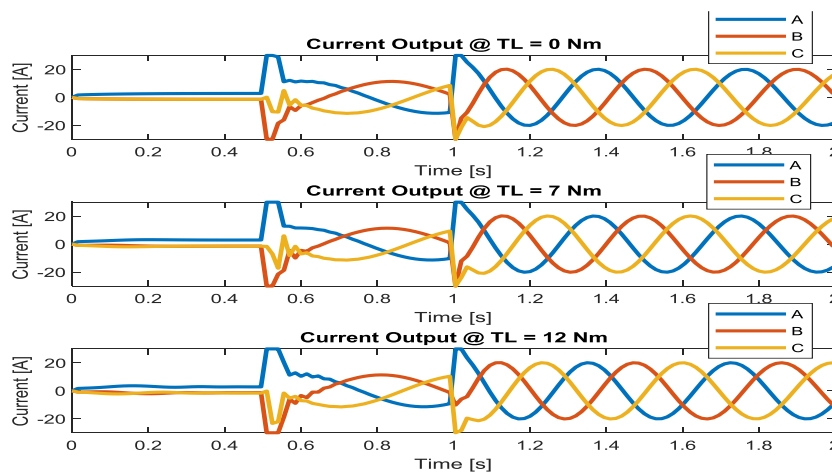


Figure 15. Torque response with FL-PID controller

**4.4 Results under variable speed and constant load torque using FL-PID-PSO controller**

The performance of the SCIM drive with a hybrid FLC-PID-PSO controller is presented in Figures 16 -18. The membership function of the fuzzy logic controller in the hybrid controller is optimized by the PSO technique, as

are the input gain parameters of the PID controller. The optimization has given an improved model, which has given an excellent result, as shown in figures 16 through 18. The model has a fast and smooth dynamic response, and the time given to switch from one reference speed to another at the desired time range is very minimal. The simulation response has shown that if the model is implemented, it will improve the efficiency of the system in terms of energy usage because there will be a massive reduction in energy loss. The speed response of Figure 16

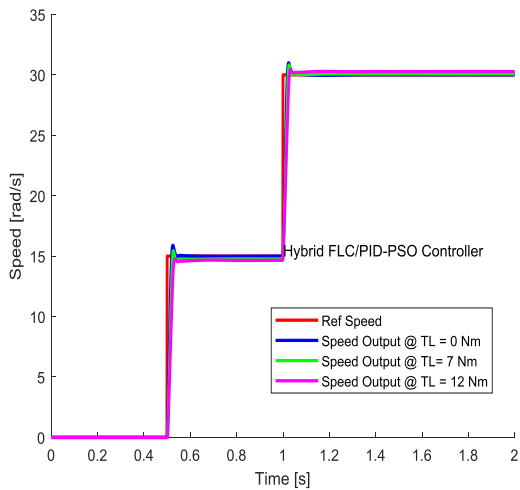


Figure 16. Current response with FL-PID-PSO controller

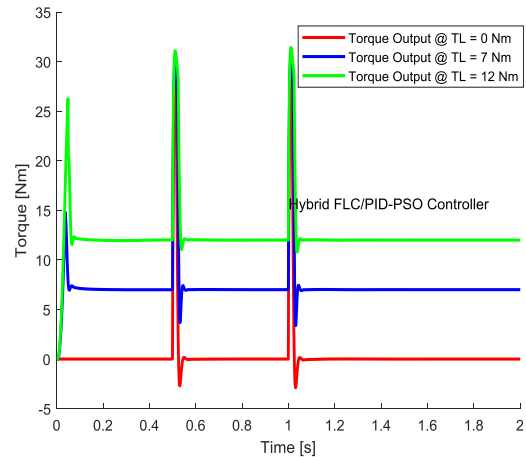


Figure 17. Current response with FL-PID-PSO controller

has an overshoot of 0.5% and an undershoot of 0%, driving 0 Nm load torque. Also, the settling time, rise time,

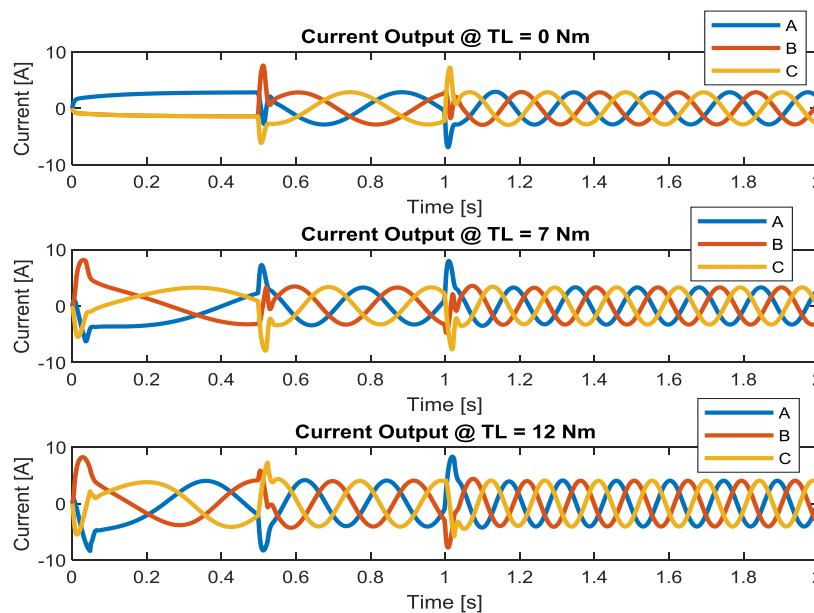


Figure 18 .Current response with FL-PID-PSO controller

Table 3. Performance comparison of controllers under variable speed and constant load torque

load	Controller	Steady State Error [rad/s]	Overshoot [%]	Settling Time [sec]	Rise Time [sec]	Undershoot [%]
0 Nm	PID	1.03	13.13	0.2	0.04	0
	FLC	0.5	10.36	0.18	0.03	0
	FLC-PID	0.2	9.87	0.17	0.026	0
	FLC-PID-PSO	0.02	0.5	0.02	0.01	0
7 Nm	PID	1.1	10.99	0.22	0.05	19.64
	FLC	1.2	8.64	0.21	0.49	8.23
	FLC-PID	0.9	8.829	0.98	0.04	7.62
	FLC-PID-PSO	0.03	0.5	0.02	0.01	0
12Nm	PID	1.2	10.99	0.33	0.04	28.356
	FLC	1.4	9.91	0.30	0.03	8.002
	FLC-PID	0.99	8.804	1.2	0.02	3.35
	FLC-PID-PSO	0.04	0.6	0.02	0.01	0

and steady state error are 0.02 sec, 0.01 sec, and 0.02 rad/s, respectively. There is an improvement in performance when compared to the dynamic performance of the motor with FLC, PID, and FLC-PID controllers under this operating condition. The corresponding electromagnetic torque and current response are shown in Figures 16 and 18, respectively. Each torque response in Figure 18 overshoots at every speed increase and settles after 0.02 s. Figure 18 shows that there is overshoot at every increase in speed and settles immediately after 0.01 s. There is a massive reduction in stator current as compared to other SCIM drive models with PID, FL, and FL-PID controllers. The comparative summary of the dynamic performance of the SCIM using the different controllers under variable speed and constant load torque is presented in Table 3.

## V. CONCLUSION

This paper presents the speed control of SCIM using vector control techniques with PID, FL, FL-PID, and FL-PID-PSO controllers. In this algorithm, the flux and torque components were controlled separately on the d-axis and q-axis through the decoupling method. The simulation results of the SCIM drive model include the stator current, rotor speed, and electromagnetic torque under constant load torque using variable speed intermittently. The speed characterization of each controller is presented using their steady state error, rise time, settling time, percentage overshoot, and undershoot. The values of these performance parameters are recorded in Table 3. From the simulation results, it is evident that the optimized hybrid controller (FL-PID-PSO) gave the best improved speed response. The model has much better speed-enhanced performance when compared to the results from [1], [13], and [27]. Also, the work has given the needed attention to SCIM low-speed analysis. The proposed model will be useful in mechatronics and robotics, where high precision and smooth speed control are paramount.

## REFERENCES

- [1] Umoette, A. T. Okoro O. I. and Davidson, I. E. "Performance Analysis of a 10hp Three phase Induction Motor Using Classical and Finite-Elements for Varying Load Conditions," 2021 IEEE PES/IAS PowerAfrica, 2021, pp.1-5.
- [2] Umoette, A. T. Okoro O. I. and Davidson, I. E "Implementation of Indirect Field Oriented Control of a 2.2kW Three-Phase Induction Motor Using MATLAB Simulink," 2021 IEEE AFRICON, 2021, pp. 1-6.
- [3] Kimiaghalam B. Rahmani M.I. and Halleh H. " Speed & Torque Vector Control of Induction Motors with Fuzzy Logic Controller " in IEEE Control, Automation and Systems, 2008, 1998, pp. 360 - 366.
- [4] Umoette, A. T. Okoro O. I. and Davidson, I. E, "Speed Performance Enhancement and Analysis of a Three Phase Induction Motor Driving a Pump Load using Vector Control Technique," 2022 IEEE PES/IAS PowerAfrica, Kigali, Rwanda, 2022, pp. 1-5, doi: 10.1109/PowerAfrica53997.2022.9905269.
- [5] Haddoun, M., Benbouzid, E.H.,Diallo, D. Abdessemed, R. Ghouili J., and Srairi, K. "Comparative analysis of control techniques for efficiency improvement in elective vehicles," in Proc. IEEE Vehicle Power Propulsion Conf., 2007, pp. 629 – 634.
- [6] A. Ingalalli, A. and Bapiraju, J.V. "Analytical model for real-time simulation of low voltage induction motor drive," in 2017 IEEE International Electric Machines and Drives Conference (IEMDC), Miami, FL, 2017.
- [7] Hussain S. and Bazaz M.A, "Review of vector control strategies for three phase induction motor drive," 2015 International Conference on Recent Developments in Control, Automation and Power Engineering (RDCAPE), 2015.

- [8] Yin, Z., Du C. J. Liu C.J., Sun X. and Y. Zhong Y., "Research on auto disturbance-rejection control of induction motors based on an ant colony optimization algorithm", IEEE Trans. Ind. Electron., vol. 65, no. 4, pp. 3077-3094, Apr. 2018.
- [9] Wang H., Yang Y., Ge X. Zuo Y. Yue Y. and Li S. "PLL- and FLL-Based Speed Estimation Schemes for Speed-Sensorless Control of Induction Motor Drives: Review and New Attempts," in IEEE Transactions on Power Electronics, vol. 37, no. 3, pp. 3334-3356, March 2022.
- [10] Amarnath K.R., "Variable Refrigerant Flow: Demonstration of Efficient Space Conditioning Technology Using Variable Speed Drives", Electric Power Research Institute (EPRI) Report 1018446, 2018.
- [11] Oliveira F. and Uki A., "Comparative Performance Analysis of Induction and Synchronous Reluctance Motors in Chiller Systems for Energy Efficient Buildings," IEEE Transactions on Industrial Informatics, vol. 15, no. 8, August 2019.
- [12] Sahu S.K., Neem D.D., "A robust speed sensorless vector control of multilevel inverter fed induction motor using particle swarm optimization," International Journal of Innovative Research in Electrical, Electronics, Instrumentation, and Control Engineering vol. 3, issue 1, January 2015.
- [13] Nazeer N., and Shahina T.N. " speed control for indirect vector control of induction motor drives at low speeds IEEE Transactions on Energy, Communication, Data Analytics and Soft Computing, pp. 1111 - 1118, sept. 2019.
- [14] Eissa M.M., Virk G.S., Abdei A.M. and Ghith E.S., " Optimum induction motor speed control technique using particle swarm optimization' International Journal of Engineering, (2013) Vol. 3, PP. 65-73.
- [15] Jayashri. W., Swapnil Z., and Rahul S., "Review of Various Methods in Improvement in Speed, Power & Efficiency of Induction Motor", IEEE Transactions on Energy, Communication, Data Analytics and Soft Computing, (2017) Vol. 5, No. 17, PP. 3293-3297.
- [16] Souad C., Latifa A., Larbi C., Aloalu C. and Said D., "Optimized torque control via back stepping using genetic algorithm of induction motor' Journal for Control, Measurement, Electronics, Computing and Communications, (2017), 57:2, PP. 379-386.
- [17] Umoette A.T, Mbetobong U. F., Ubom E.A., "Development of Site-Specific Optimal Tilt Angle Model for Fixed Tilted Plane PV Installation in Akwa Ibom State, Nigeria". *Science Journal of Energy Engineering*. Vol. 4, No. 6, 2016, pp. 50-55. doi: 10.11648/j.sjee.20160406.11
- [18] Umoette A. T, Ubom E.A. Akpan I. E. "Comparative Analysis of Three NOCT-Based Cell Temperature Models". *International Journal of Systems Science and Applied Mathematics*. Vol. 1, No. 4, 2016, pp. 69-75. doi: 10.11648/j.ijssam.20160104.16
- [19] Umoette A.T, Udofia J. P. and Ubom E.A., "Energy Audit and Standalone Solar Power Generation Design For Akwa Ibom State University Main Campus". *International Multilingual Journal of Science and Technology (IMJST) ISSN: 2528-9810* Vol. 8 Issue 6, June – 2023
- [20] Ali A, Hannan J., Mohamed A.," A Novel Quantum-Behaved Lightning Search Algorithm Approach to Improve the Fuzzy Logic Speed Controller for an Induction Motor Drive". *Energies* 2015, 8, 13112-13136.
- [21] Hannan M.A., Ali J. A., Mohamed A., Amirulddin U. A. U, Tan N. M. L and Uddin M. N., "Quantum-Behaved Lightning Search Algorithm to Improve Indirect Field-Oriented Fuzzy-PI Control for IM Drive," in IEEE Transactions on Industry Applications, vol. 54, no. 4, pp. 3793-3805, July-Aug. 2018.
- [22] Blashke F., "The principle of field orientation as applied to the new transvector closed loop control system for rotating field machines", *Siemens Rev*, Vol 39, no.5, pp 217-220, May 1972.
- [23] Stephen O., Ejirofor N., Abuch N.Ci , Damian N. , Okoro O. I. "Performance study of three-phase induction motor driving a load". *ANALYSIS ARTICLE DISCOVERY ISSN 2278-5469 EISSN 2278-5450 A* 2019.
- [24] Bhola J., Panda M., Pandey P.K, and Pan Lt. " PSO-Based Online Vector Controlled Induction Motor Drives." IEEE International Conference on Electrical, Electronics, and Optimization Techniques (ICEEOT) - 2016: 2234-2240.
- [25] Fattah J.A. and Ikhliss, P.E. " Performance and Comparison Analysis of Speed Control of Induction Motors using Improved Hybrid PID-Fuzzy Controller." *CES Transactions on Electrical Machines and Systems* 2, no. 2 (2015): 575-581.
- [26] Zicheng, L., yongdong L. , and Zheng Z. ,"A review of drive techniques for multiphase machines." *CES Transactions on Electrical Machines and Systems* 2, no. 2 (2018): 243-251.
- [27] Tiwari R. and Chatterji S., "Comparative Analysis of Vector Control of Induction Motor using PI Controller with Fuzzy Logic Controller." *International Journal of Science and Research (IJSR)*, vol. 2, no. 4, pp. 404-409, April 2013.
- [28] Goman V., Prakht V., Kazakbaev V. and Dmitrievskii V. "Comparative Study of Induction Motors of IE2, IE3 and IE4 Efficiency Classes in Pump Applications Taking into Account CO2 Emission Intensity" *Applied Sciences* 2020. MDPI.
- [29] Ukut, U. I., Umoette A.T and Okpura, N., "Fast Decoupled Load Flow Analysis of IEEE 33 Bus Distribution System". *Journal of Multidisciplinary Engineering Science Studies (JMESS) ISSN: 2458-925X* Vol. 9 Issue 1, January – 2023.
- [30] Silas A. F., Offiong N.S, and Umoette A.T., "Power Transfer Capability Enhancement on Nigeria 330KV Lines Using Unified Power Flow Controller (Facts Device)". *Journal of Multidisciplinary Engineering Science and Technology (JMEST) ISSN: 2458-9403* Vol. 10 Issue 2, February – 2023
- [31] Singha A.K., Chaturvedib D.K. and Palc N.K, "PSO based Fractional Order PID Controller for Speed Control of Induction International Conference on Power Energy", *Environment and Intelligent Control (PEEIC)* 2019.
- [32] Yang Z., Lu C., Sun X., Ji J. and Ding Q., "Study on Active Disturbance Rejection Control of a Bearingless Induction Motor Based on an Improved Particle Swarm Optimization-Genetic Algorithm," in IEEE Transactions on Transportation Electrification, vol. 7, no. 2, pp. 694-705, June 2021.
- [33] Jha B., Panda M. K., Pandey P. K, Pant L., "PSO-Based Online Vector Controlled Induction Motor Drives". *International Conference on Electrical, Electronics, and Optimization Techniques (ICEEOT) – 2016*
- [34] Cheng S., Gong B., Wang J. A, "Novel Hybrid Speed Controller of the Vector Control System", *International Conference on Control, Automation and Systems* 2010, Oct. 27-30, 2010 in KINTEX, Gyeonggi-do, Korea.
- [35] H. Mohan M. K. Pathak, and Dwivedi S.K., "Reactive Power Based Speed Control of Induction Motor Drive using Fuzzy Logic for Industrial Applications". *IEEE International Conference on Power Electronics, Smart Grid and Renewable Energy (PESGRE2020)*. 2020.
- [36] Dedid C.H. and Ardik W. "Implementation of genetic algorithm for parameter tuning of PID controller in three-phase induction motor speed control", *IPTEK, Journal of Engineering*, Vol.1, No. 1. PP. 715 – 719. 2014
- [37] Rami A., Maher I., Walid E. and Mahmoud A., "Indirect Field Oriented Control of an Induction Motor Sensing DC-link Current with PI Controller". *International Journal of Control Science and Engineering* 2012, 2(3): 19-25 DOI: 10.5923/j.control.20120203.01. PP. 19-25.
- [38] Ahmad I. and Tripathi R.K., "Indirect field-oriented control (IFOC) of induction motor using SPVPWM fed with Z-source inverter". *IEEE conference on Engineering and system*, PP 1.5. 2012

- [39] Silas A. F., Umoette A.T., and Ekanem B.D. “Energy Analytical Model for The Selection of Peak Sun Hour and Days of Power Autonomy for PV Solar Power System Components Sizing”. *Journal of Multidisciplinary Engineering Science and Technology (JMEST)* ISSN: 2458-9403 Vol. 11 Issue 3, March – 2024
- [40] Umoette A.T., Silas A. F. and Kingsley B. C. “Clearness Index–Based Computation and Evaluation of Mean Daily Insolation and Optimal Fixed Tilt Angle for PV Installation in Uyo, Akwa Ibom State”. *International Multilingual Journal of Science and Technology (IMJST)* ISSN: 2528-9810 Vol. 9 Issue 3, March – 2024
- [41] Madhavi L. and Mhaisgewal S.i, “Induction motor speed control using PID controller” *International Journal of Technology and Engineering Science*, Vol. 1 (2), PP. 151-155. 2013.
- [42] Pravallika S., Chandra J.N. and Reddy D.P. “Optimization of speed control of induction using self-tuned PI plus hybrid controller”. *Internation journal of emerging technology and advanced engineering*, Vol. 5, Issue 1. 2015
- [43] Silas A. F., Kingsley B. C. and Umoette A.T. “Sun Chart-Based Computation of Photovoltaic Array Row Spacing for Internal Shading Mitigation at Optimal Fixed Tilt Angle”. *Journal of Multidisciplinary Engineering Science and Technology (JMEST)* ISSN: 2458-9403 Vol. 11 Issue 3, March – 2024
- [44] Umoette A.T., Liberty S. and Effiong F.E. “Development of A Fuzzy Logic-Based Mechanism for Enhancement of Power Generation System Stability”. *International Multilingual Journal of Science and Technology (IMJST)* ISSN: 2528-9810 Vol. 7 Issue 5, May – 2022